Reprinted from SPIE Vol. 925—Ocean Optics IX

Finite-Difference Evolution of a Scattered Laser Pulse in Ocean Water

J. Tessendorf, C. Piotrowski, R.L. Kelly

Areté Associates
P.O. Box 6024
Sherman Oaks, CA, 91413

ABSTRACT

The propagation of a finite-sized laser pulse through ocean water is simulated. In-water absorption and scattering are included in the simulation by using an explicit finite-difference formulation of the evolution equation equivalent to the time-dependent radiative transfer equation. The finite-difference scheme assumes that the time step is sufficiently small that the distance the light travels in one step is less than one scattering length. It also includes a causal interpolation algorithm which insures that the observed speed of light is equal to the physical speed to within the spatial and temporal resolution of the calculation. It is shown that the scheme is stable regardless of the grid geometry. With only a few restrictions connecting the spatial, angular, and temporal grids, it is also consistent. As guaranteed by Lax's theorem, the consistency and stability of this scheme imply that the finite-difference solution converges to the continuous solution as the grids become dense. The propagation, absorption, and scattering of a cylindrically symmetric pulse are shown, and the spread of the pulse is calculated from the simulation.

1. INTRODUCTION

There is increasing interest in the use of pulsed laser beams in the ocean, for example, in bottom mapping by airborne laser hydrography[1], or in high-bandwidth underwater communications. The operational success of such applications is limited by the extent of "pulse stretching" and other multiple scattering effects, as well as absorption. In

order to assess scattering and absorption degradation on particular designs, it is useful for system design and performance engineers to have available analytic models of such effects. Analytical expressions for pulse broadening have been constructed using small-angle approximations and equivalencing range with propagation time[2], but these two assumptions are severely limited in predictive ability of the evolution of the full light field. Monte Carlo methods have been used to extract pulse properties in both water and clouds[3], but these results have not been reduced to models of the radiance field. In addition, it may be difficult to calculate a full radiance field over a large volume with good Monte Carlo statistics.

The aim of the efforts outlined below is to develop such models. The approach is a combination of numerical and analytic methods for obtaining the spatial and angular distribution of radiance of a pulse as it evolves in time. A finite-difference code for the radiance distribution has been developed and is the principal subject of discussion in the remaining sections. The algorithm on which this code is based exhibits several advantages over finite-difference codes developed by others[4], including unconditional stability and propagation of light at only the physical speed. The numerical results from these calculations can act as numerical experiments which can be compared with analytic models under consideration. A particular model discussed below was obtained from a non-rigorus approximate evaluation of a path integral expression for the evolution operator satisfying the time-dependent radiative transfer (TDRT) equation.

The starting point of both the numerical and analytic approaches is with the evolution operator defined in the next section. All solutions of the TDRT equation can be obtained from the evolution operator and the initial radiance distribution, which is why it is natural to formulate the solution in this fashion. The evolution operator is formally identical to the "radiative process" introduced by Preisendorfer[5].

2. FINITE-DIFFERENCE EVOLUTION ALGORITHM

The TDRT equation for the radiance $L(s,\vec{x},\hat{n})$ at time s, position $\vec{x}$, and in direction $\hat{n}$ is

$$\{\frac{\partial}{\partial s} + \hat{n}.\nabla + c\}\, L(s,\vec{x},\hat{n}) = b\int P(\hat{n},\hat{n}')\, L(s,\vec{x},\hat{n}')\, d^2 n'$$

where c is the total attenuation coefficient, b is the scattering coefficient, and $P(\hat{n},\hat{n}')$ is the unit-normalized phase function. The time s is measured in units of length with s=vt, where t is time measured in seconds and v is the speed of light in the ocean (~ 2.3×10^8 m/s). A formal solution of this equation can be written in terms of a space and angle convolution of an evolution operator with the initial distribution:

$$L(s,\vec{x},\hat{n}) = \int d^3x' d^2n'\; G(s,\vec{x}-\vec{x}',\hat{n},\hat{n}')\; L_o(\vec{x}',\hat{n}'), \quad (2)$$

where $G(s,\vec{x}-\vec{x}',\hat{n},\hat{n}')$ is the evolution operator and $L_o(\vec{x}',\hat{n}')$ is the initial distribution. This is equivalent to the finite-difference scheme

$$L(s+\Delta s,\vec{x},\hat{n}) = \int d^3x' d^2n'\; G(\Delta s,\vec{x}-\vec{x}',\hat{n},\hat{n}')\; L(s,\vec{x}',\hat{n}'). \quad (3)$$

The development of a finite-difference algorithm based on equation 3 which is suitable for numerical implementation is described by Tessendorf.[6] A partition of the unit sphere must be chosen, providing a finite set of directions of propagation $\{\hat{n}_k\}$, k = 1,...,N, and a corresponding set of solid angles $\{\Delta\Omega_k\}$ such that

$$\sum_{k=1}^{N} \Delta\Omega_k = 4\pi.$$

Restricting the size of the time step to be smaller than one scattering length ($\Delta s << 1/b$) allows an approximation of the expression for the bin-averaged evolution operator G. The resulting algorithm is

$$L_k(s+\Delta s,\vec{x}) = \exp(-c\Delta s) \sum_{k'=1}^{N} T_{kk'}(\Delta s)\, L_{k'}(s,\vec{x}-\hat{n}_{k'}\Delta s). \quad (4)$$

The elements of the transition matrix **T** are

$$T_{kk'} = \exp(b\Delta s\mathbf{P})_{kk'} \tag{5}$$

where the elements of the phase matrix **P** are

$$P_{kk} = \frac{1}{\Delta\Omega_k} \int_k d^2n \int_{k'} d^2n' P(\hat{n},\hat{n}'). \tag{6}$$

The radiance $L_K(s,\vec{x})$ is an average over bin k:

$$L_k(s,\vec{x}) = \frac{1}{\Delta\Omega_k} \int_k d^2n\ L(s,\vec{x},\hat{n}).$$

A complete numerical algorithm follows from equation 4 once a set of spatial grid points $\{\vec{x}_i\}$ and an interpolation scheme for estimating the radiance at the points $\vec{y}_{ik} = \vec{x}_i - \hat{n}_k\Delta s$ are chosen. As demonstrated by Tessendorf,[6] this algorithm is unconditionally stable. When an appropriate interpolation is used, the original TDRT equation is reproduced as the spatial, angular, and temporal grids become arbitrarily dense, i.e., the algorithm is consistent. From Lax's theorem[7], the solution from this algorithm converges to the continuous solution. There is considerable freedom in choosing the spatial grid relative to the partition of the unit sphere and the time step[6], but the interpolation algorithm must be chosen carefully to insure the correct speed of propagation.

Most interpolation schemes allow the radiance to propagate at a speed faster than the physical speed of light. The reason for this is that interpolation using points surrounding the point $\vec{x}_i - \hat{n}_k\Delta s$ usually includes points which lie at a distance greater than Δs from $\vec{x}_i$. Consequently, in a single time step radiance travels more than Δs, which produces acausal behavior. The problem is eliminated by using the following set of steps, called "causal interpolation" (CI):

(a) A position-, direction-, and time-dependent length scale $\ell_{ik}(s)$ is defined which replaces the time step length Δs in the interpolation formula. The modified algorithm is

$$L_k(s+\Delta s,\vec{x}_i) = \exp(-c\Delta s) \sum_{k'=1}^{N} T_{kk'}(\Delta s) \times L_{k'}(s,\vec{x}_i - \hat{n}_k,\ell_{ik}(s)) \qquad (7)$$

(b) Choose the interpolation point $\vec{x}_{ikl}(s)$ from the set of points within a distance $\ell_{ik}(s)$ of $\vec{x}_i$, and within the angular bin Ω_k. Generate the weights $\omega_{ikl}(s)$ and interpolate the radiance. Typically, the set of points and weights used varies from time step to time step.

(c) Find the distance

$$\delta_{ik}(s) \equiv \max_l \{|\vec{x}_i - \vec{x}_{ikl}(s)|\},$$

which is the greatest distance light traveled in the direction $\hat{n}_k$ to reach $\vec{x}_i$ during this time step.

(d) Update ℓ_{ik} to the next time step by the procedure

$$\ell_{ik}(s+\Delta s) = \ell_{ik}(s) + \Delta s - \delta_{ik}(s).$$

(e) A time step index $m_{ik}(s)$ is defined to account for situations in which no points except $\vec{x}_i$ are found for the interpolation. $m_{ik}(s)$ is equal to the number of time steps backward the distribution must be sampled. For situations in which points in addition to $\vec{x}_i$ were found in the previous time step, $m_{ik}(s) = 1$. If no points in addition to $\vec{x}_i$ were found, $m_{ik}(s) = m_{ik}(s-\Delta s)$

+ 1. Equation 7 is the algorithm used when $m_{ik'}(s) = 1$. For larger values, the algorithm is generalized to

$$L_k(s+\Delta s, \vec{x}) = \sum_{k'=1}^{N} \exp\{-c m_{ik'}(s)\Delta s\}\, T_{kk'}(m_{ik'}, \Delta s) \times L_{k'}(s-(m_{ik'}-1)\Delta s, \vec{x}_i - \hat{n}_{k'}\ell_{ik'}(s))$$

The consistency of the finite-difference algorithm is maintained under CI because $\Delta s < \ell_{ik}(s) < \Delta s + \sigma_{ik'}$ where σ_{ik} is the local grid spacing, so that $\ell_{ik} \to \Delta s$ as $\sigma_{ik} \to 0$, restoring the original finite-difference algorithm. After m time steps, the apparent speed in direction $\hat{n}_k$ at $\vec{x}_i$ is

$$v_{ik}^{app}(s) = 1 + 0\left(\frac{\sigma_{ik}}{s}\right),$$

where $s=m\Delta s$, so that the apparent speed of light resulting from this algorithm is the physical speed plus a term which vanishes with time.

3. THE CALCULATION

The finite-difference algorithm described in the previous section was coded and executed in FORTRAN on a VAX 11/785 for the propragation of a cylindrically symmetric pulse through 100 meters of ocean with no absorption (a=0), a scattering coefficient $b=0.1m^{-1}$, and a phase function obtained by a piecewise fit to Petzold's data[8] (see Figure 1). Cylindrical symmetry is the property that the radiance distribution is invariant when the spatial and directional azimuthal angles are rotated rigidly together. If the propagation direction is given by the angle (θ,ϕ) in spherical coordinates, and the position by (ρ,Φ,z) in cylindrical coordinates, then the symmetry is

$$L(s,\rho,\Phi,z,\theta,\phi) = L(s,\rho,\Phi+\Delta,z,\theta,\phi+\Delta). \qquad (10)$$

The FORTRAN code obtains the radiance in the plane $\Phi=0$ at each time step. This requires knowledge of the radiance at non-zero spatial azimuths in each previous time step, which is obtained using equation 10. The unit sphere was partitioned into 26 direction bins, with an equi-angular division of θ into 5 regions, and an equi-angular division of ϕ into 8 regions for the bins away from $\theta=0^{o}$ and 180^{o}. The spatial grid in the $\Phi=0$ plane is rectangular, with grid spacing $\Delta\rho = \Delta z = 1m$. Initially, the number of points in the ρ- and z- directions is $N_{\rho} = 11$ and $N_{z} = 10$. As the pulse propagates, the grid expands in the z-direction to a maximum of $N_{z} = 102$. The initial distribution of the pulse has energy in the forward direction bin only, at the single grid point at z = 1m on the z-axis, the axis of propagation. The evolving distribution was obtained for 95 time steps, which required about 15 hours of cpu time and 3/4 Mbyte of memory on the VAX 11/785.

Contour plots of the resulting distribution in the forward direction in the (ρ,z) plane at several times are presented in Figure 2. The contour levels have a maximum value of $.1L_{o}$, where L_{o} is the initial pulse strength, and decrease by a factor of 10 to a minimum of $10^{-6}\ L_{o}$. If causal interpolation had not been used, the edge of the distribution would have the shape of a square, with the sides moving at the physical speed of light in the ρ- and z- directions, and the corners of the square propagating faster than the physical speed.

4. MODELING

The development of analytic models for the radiance distribution based on numerical work such as described in the previous sections is in its initial stages. Two approaches have been examined: (1) a phenomenological method in which the numerical data is searched for patterns which can be expressed in analytic form; (2) a highly theoretical method using approximate evaluation of a path integral expression, the result of which could be compared with the numerical data to fix a constant in the evaluation and to determine the conditions of validity of the approximation. From the preliminary results

presented here, these two approaches appear to be complementary in that the phenomenological method is useful for modeling the development of the distribution in the region near the pulse, and the approximate theoretical method gives the distribution many scattering lengths behind the pulse.

The common theme in both approaches is to concentrate on developing analytic expressions for the evolution operator. The initial distribution of the calculation in Section 3 approximates a point distribution to within the resolution of the grids, so the distribution at later times should correspond to that of the evolution operator in a cylindrical geometry.

In the context of the phenomenological approach, Figure 3 is a plot of the maximum value of the radiance at each time in the forward-direction (k=1). The peak attenuates in a simple exponential way

$$L_{peak}(s) \sim L_{peak}(o)\ e^{-K_p s}, \qquad (11)$$

with $K_p \sim 0.0262\ m^{-1}$. Calculations with several choices of values for a and b show that this attenuation coefficient can be written as

$$K_p = a + b(1-P_{11}), \qquad (12)$$

This expression is exactly what would be expected if multiple-scattering could be ignored, since the finite-difference equation in the forward direction would become

$$L_1(s + \Delta s, \vec{x}) \sim e^{-K_p \Delta s}\ L_1(s, \vec{x} - \hat{n}_1\ \Delta s).$$

This result implies that energy radiates from the propagating "core" by single-scattering, with multiple-scattering important only in the region behind the pulse.

Figures 4 and 5 illustrate the evolution of the radiance distribution at the initial position from a single scattering behavior to a multiple-scattering one. The angular distribution after one time step mimics that of the phase function (compare the relative magnitudes of the forward and backward values in Figure 4). With time however, the relative magnitudes of the radiance in each direction converge, as depicted in Figure 5. (The oscillations in the 45^{o} and 135^{o} directions in Figure 5 are due to the causal interpolation procedure, and are damped with time as the spatial distribution becomes uniform. They can also be suppressed by using a densor spatial grid. The oscillations will never grow beyond their amplitude at early times because the finite-difference algorithm is unconditionally stable.) A general rule of thumb which follows is that at great distances behind the pulse, the distribution become relatively insensitive to angle.

The "theoretical" approach is an attempt to approximately solve the TDRT equation for the evolution operator. Perkins solved the TDRT equation in the small-angle approximation[9]. That solution predicts, however, that the angular distribution is always sensitive to angle. The method adopted here begins with a path integral representation of the evolution operator described in the Appendix of Reference 6. An approximate evaluation of the path integral has been obtained in the form

$$G(s,\vec{x}-\vec{x}',\hat{n},\hat{n}') = G_o(S)\ (\mu bC(s))^{-3/2} e^{-A(s)}\, e^{\hat{n}\cdot\hat{n}'B(s)}$$

$$+ \exp\left\{ -\frac{1}{\mu bC(s)}\ (\vec{x} - \vec{x}' - (\hat{n} + \hat{n}')D(s))^2 \right\},$$

with

$$G_o(s) = \left(2\pi\ \frac{\sinh/\omega_c s}{\omega_c}\right)^{-3/2}$$

$$A(s) = \frac{\omega_c \sinh(2\omega_c s)}{2\mu b \sinh^2(\omega_c s)}$$

$$B(s) = \frac{\omega_c}{\mu b} \quad \frac{1}{\sinh(\omega_c s)}$$

$$C(s) = [\omega_c{}^3 \sinh(\omega_c s)]^{-1} \left\{ (\omega_c s)\sinh(\omega_c s) + 2(1 - \cosh(\omega_c s)) \right\}$$

$$D(s) = [\omega_c \sinh^2(\omega_c s)]^{-1} \; [(\omega_c s)\; (\cosh(\omega_c s) - 1)].$$

The approximations required to obtain this expression are:

1. The phase function includes only forward scattering, with a mean-square width μ defined by

$$\mu = 2\pi \int_o^\pi d(\cos\theta)\, \sin^2\theta\, P(\theta).$$

For ocean water $\mu \sim .03$

2. The magnitude $|\vec{x} - \vec{x}'| < s$, although a more precise statement of the range of validity of the expression will have to be obtained from numerical data.

In particular, this expression does not assume a small-angle approximation. The constant $1/\omega_c$ is a diffusion length arising from the approximation, and must be determined from numerical data. The reason it is indefinite is that this expression is not a correct approximate evaluation of the path integral. Instead ω_c should be a function of time. Nevertheless this expression could be reasonable at positions

sufficiently far behind the pulse that the angular distribution is dominated by many forward-scattering events. The predicted angular distribution at the initial position is

$$G(s,0,\hat{n},\hat{n}') \propto \exp\left\{ -(1-\hat{n}\cdot\hat{n}') \left[B(s) - \frac{D^2(s)}{\mu bC(s)}\right]\right\},$$

which becomes insensitive to angle when $s >> 1/\omega_c$. More numercial work is needed to determine the value of ω_c and the ranges of $\vec{x} - \vec{x}'$ and s over which the expression is valid.

5. CONCLUSIONS

The finite-difference algorithm and code presented here has two properties not available in other algorithms or codes: unconditional stability (i.e., independent of choice of grids), and propagation of the radiance distribution at the correct physical speed in all directions at all positions. It does suffer from the ray effects found in other algorithms that partition the propagation directions (θ,ϕ) into discrete bins. Nevertheless the numerical experiments which can be generated should prove useful in the development of new models of in-water pulse propagation.

ACKNOWLEDGEMENTS

The preparation of this manuscript and calcuations presented within were supported by Arete Associates. We would like to thank Shirl Miklas for typing the manuscript.

REFERENCES

1. G.C.Guenther and R.W.L. Thomas, "Effects of Propagation-induced Pulse Stretching in Airborne Laser Hydrography", SPIE Vol. 489, Ocean Optics VII, 287 (1984).

2. L.B. Stotts, "Closed Form Expression for Optical Pulse Broadening in Multiple-Scattering Media", Appl. Optics 17, 504, (1978); J.W. McLean, D.R. Crawford, C.L. Hindman, "Limits of Small Angle Scattering Theory", Appl. Optics 26, 2053, (1987).

3. R.M. Lerner and J.E. Summers, "Monte Carlo Description of Time- and Space- Resolved Multiple Forward Scatter in Natural Water", Appl. Opt. 21, 861 (1982); E.A. Bucher, "A Computer Simulation of Light Pulse Propagation for Communication Through Thick Clouds", Appl. Opt. 12, 2391 (1973).

4. R.D. Richtmyer and K.W. Morton, Difference Methods for Initial-Value Problems, (John Wiley and Sons, New York, 1967); K.D. Lathrop, R.E. Anderson, and F.W. Brinkley, "TRANZIT: A Program For Multigroup Time-Dependent Transport in (ρ,z) Cylindrical Geometry", Los Alamos Scientific Laboratory Report LA-4575 (1971).

5. R.W. Preisendorfer, Radiative Transfer on Discrete Spaces, (Pergoman Press, New York, 1965).

6. J. Tessendorf, "Time-Dependent Radiative Transfer and Pulse Evolution", (1988), submitted to JOSA A.

7. E. Isaacson and H.B. Keller, Analysis of Numerical Methods, (John Wiley and Sons, New York, 1966).

8. T.J. Petzold, "Volume Scattering Functions for Selected Ocean Waters", SIO/VisLab Reference 72-78; (1972).

9. F.W. Perkins, "A Radiative Transfer Model for Undersea Optics Applications", JSR-82-107 (1982).

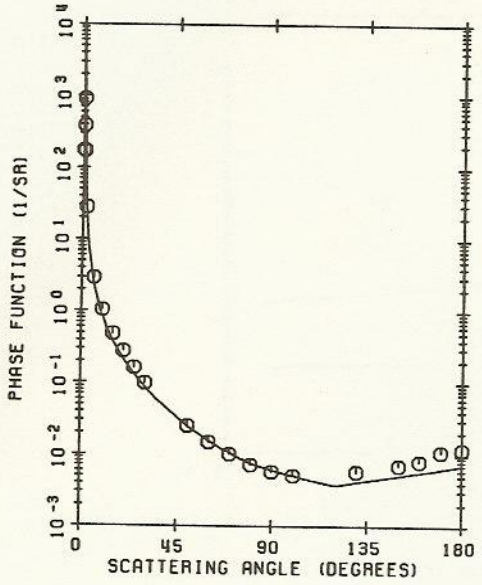

Figure 1: Data and piecewise fit for the phase function. The data are from reference (8), station 9, test 161, 14 July 1971.

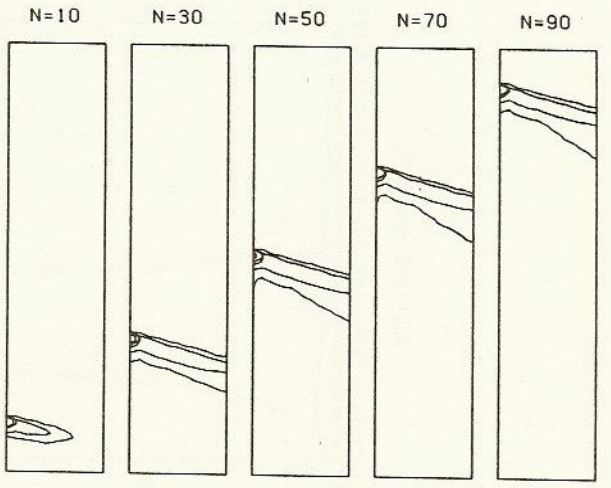

Figure 2: Contour plots of the radiance distribution in the (ρ, z) plane in the forward (k=1) direction, at times s=10,30,50,70,90 meters.

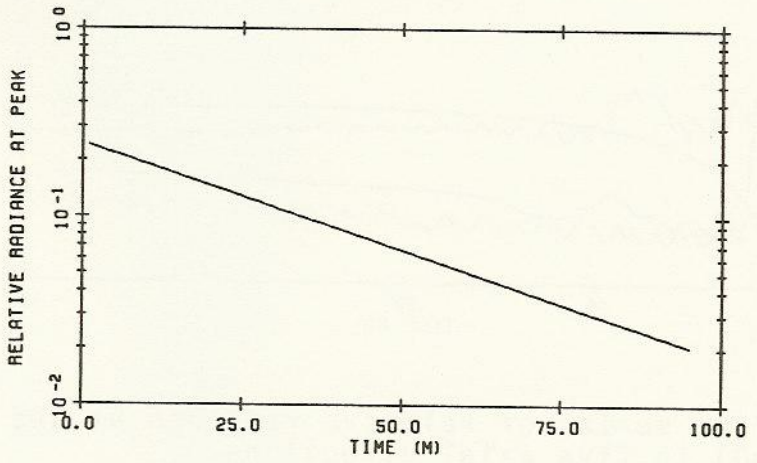

Figure 3: Maximum radiance in the forward (k=1) direction for each time step.

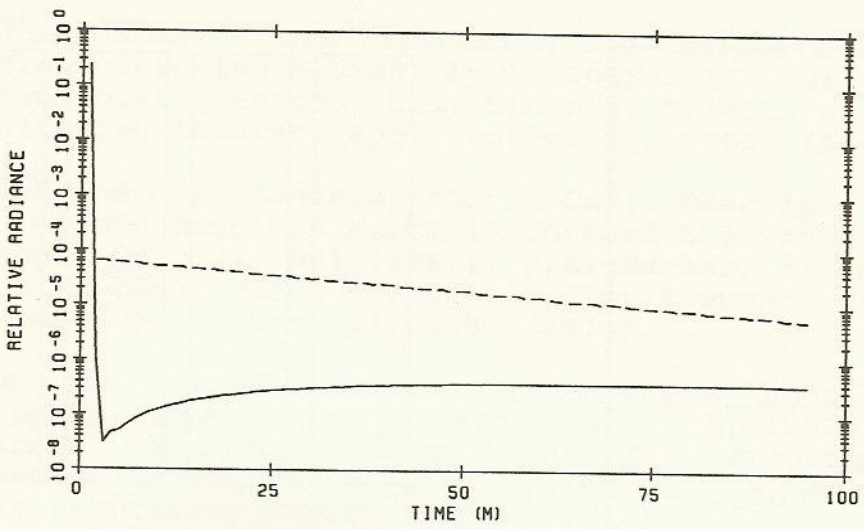

Figure 4: Time series of relative radiance at the initial position (z=0) in the forward (solid) and backward (dash) directions.

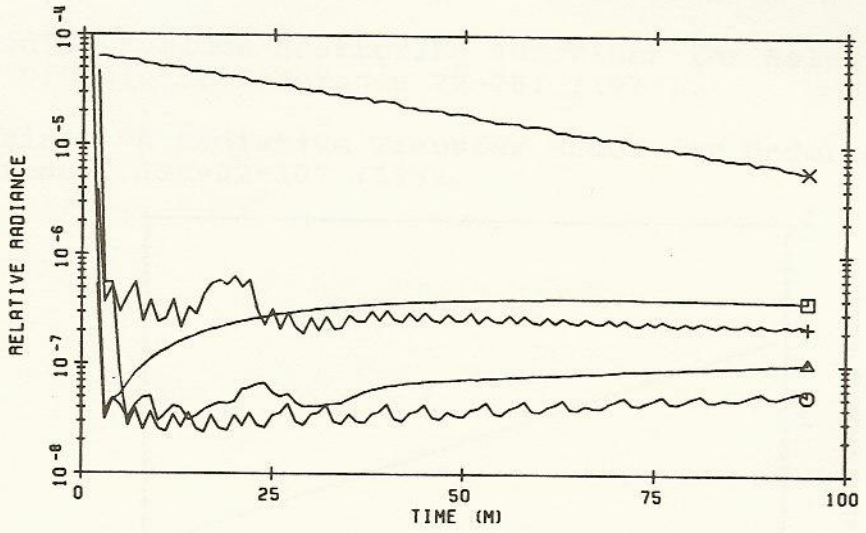

Figure 5: Time series of relative radiance at the initial position (z=0) in five axial directions.
⊡:θ = 0°; o:θ = 45°; Δ:θ = 90°; +:θ = 135°; ×:θ = 180°.